Accepted Manuscript

Check for updates

Journal of
Materials Chemistry C

Materials for optical, magnetic and electronic devices

rsc.li/materials-c

Volume 6
Number 5
7 February 2018
Pages 911-1266

ISSN 2050-7526

ROYAL SOCIETY OF CHEMISTRY

PAPER
Nosang V. Myung, Yong-Ho Choe et al.
A noble gas sensor platform: linear dense assemblies of single-walled carbon nanotubes (LACNTs) in a multi-layered ceramic/metal electrode system (MLES)
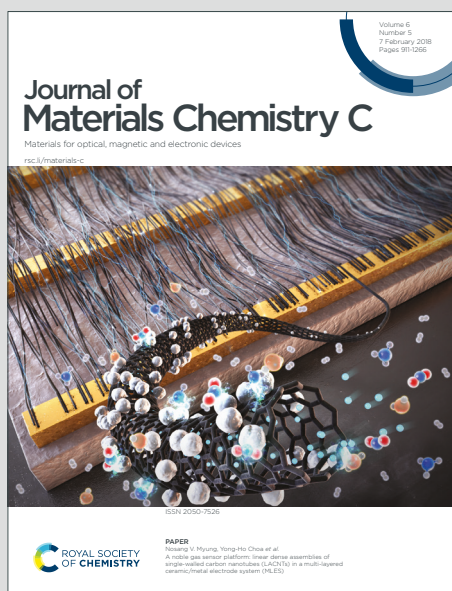
This is an Accepted Manuscript, which has been through the Royal Society of Chemistry peer review process and has been accepted for publication.

Accepted Manuscripts are published online shortly after acceptance, before technical editing, formatting and proof reading. Using this free service, authors can make their results available to the community, in citable form, before we publish the edited article. We will replace this Accepted Manuscript with the edited and formatted Advance Article as soon as it is available.

You can find more information about Accepted Manuscripts in the Information for Authors.

Please note that technical editing may introduce minor changes to the text and/or graphics, which may alter content. The journal's standard Terms & Conditions and the Ethical guidelines still apply. In no event shall the Royal Society of Chemistry be held responsible for any errors or omissions in this Accepted Manuscript or any consequences arising from the use of any information it contains.

ROYAL SOCIETY OF CHEMISTRY

rsc.li/materials-c

ARTICLE

Nanostructured Copper Sulfide Thin Film *via* a Spatial Successive Ionic Layer Adsorption and Reaction Process Showing Significant Surface-Enhanced Infrared Absorption of CO₂

Yujing Zhang,[a] Xinyuan Chong,[b] Hao Sun,[a] Muaz M. Kedir,[a] Ki-Joong Kim,[c,d] Paul R. Ohodnicki,[c] Alan Wang[b] and Chih-hung Chang*[a]

Infrared (IR) imaging gas sensing technique is excellent for CO₂ gas detection systems that require high accuracy and safety standard; however, there is a significant barrier in application due to its high cost and difficulty in miniaturization. CO₂ sensors that are functional within near- or short-wavelength IR have the potential to reduce this barrier. In this work, a highly sensitive plasmonic material based on nanostructured covellite copper sulfide (CuS), which exhibits desired localized surface plasmon resonance for surface-enhanced IR absorption (SEIRA) throughout near- and mid-IR ranges, was investigated. We prepared CuS thin films facilely in an additive manner based on a spatial successive ionic layer adsorption and reaction process at room temperature. The resulting CuS thin film possesses a structure consisting of hexagonal nanoflakes, and demonstrates significant SEIRA for 100-ppm CO₂ with an enhancement factor of 10^4.

Introduction

CO₂ is one of the most important greenhouse gases that contributes to over 80% of greenhouse gas emissions in the United States, of which the concentration has increased globally by 45% in the past two hundred years (IPCC 2013; NOAA/ESRL 2018a, 2018b, 2018c). In spite of the significant advances of many renewable energies with low carbon emission, fossil fuels remain as the primary energy resources of human activities. The increasing CO₂ level in the atmosphere as one of the main effects of burning fossil fuels contributes to substantial environmental impacts[1]. To better serve CO₂ emission mitigation strategies, it is crucial to develop efficient sensing techniques for CO₂ that can function at the source of emissions such as the use of fossil fuels in transportation, electricity generation or industrial processes. Many new sensing technologies have been developed to monitor CO₂ levels under different conditions[2-10]. Among all, Fourier-transform infrared (FTIR) spectrometer is ideal for gas detection systems that require high sensitivity and accuracy. Conventional FTIR spectrometer is bulky and expensive, which is not suitable for low-cost distributed sensing. Thus, there is a strong need to develop new approaches for low-cost and distributable spectroscopy-based sensing for CO₂. Commonly-used IR gas sensors for CO₂ detection operate at mid-infrared (MIR) wavelength because the absorption bands of CO₂ in both the near-infrared (NIR) and the short-wavelength infrared (SWIR) ranges are typically weak[11], which becomes an even greater hindrance in practical sensing application where usually only a small amount of gas molecules is present. Developing CO₂ sensors that are functional at NIR/SWIR wavelength will enable the development of low-cost, chip-scale IR sensors and allow for the use of commercially available optical fibres for distributed sensing[12].

One promising development to improve this situation is through surface-enhanced infrared absorption (SEIRA)[13] by integrating plasmonic materials with compatible sensing platforms. Localized surface plasmon resonance (LSPR) is capable of enhancing the absorption, and meanwhile, providing rapid and label-free sensing[14, 15]. There are several reports regarding the study of LSPR-enhanced CO₂ gas sensors, among which metals[16-29] and metal oxides[30], especially gold, silver, and transparent conductive oxide, are the most popular plasmonic materials due to their outstanding LSPR in visible/NIR range. The defined and intense LSPR absorption of these materials is highly dependent on their crystal structure, micro- and nanostructure, and morphology[31-34]. Therefore, it is common that sophisticated synthesis and processing routes are used to fabricate these sensors for precise micro/nanostructure control. Typically, the plasmonic-material thin films are prepared by thermal evaporation[19], sputtering technique[24], or post-processing of nanoparticles[27, 30]. To obtain enhanced LSPR

[a.] School of Chemical, Biological Environmental Engineering, Oregon State University, Corvallis, OR 97331, USA.

[b.] School of Electrical Engineering and Computer Science, Oregon State University, Corvallis, OR 97331, USA.

[c.] National Energy Technology Lab, United States Department of Energy, Pittsburgh, PA 15236, USA.

[d.] LRST, Pittsburgh, PA 15236, USA.

* Corresponding author. Email address: chih-hung.chang@oregonstate.edu

ARTICLE

Journal Name

absorption, fabrication of plasmonic materials in precisely controlled micro/nanostructures is needed. For this reason, sophisticated techniques are frequently used for the fabrication of plasmonic devices, such as hole-mask colloidal lithography[20], photolithography[22], nanosphere lithography[17], focused ion beam nanofabrication[28, 29], pulse laser deposition[31], electron beam lithography[32], etc.

The change based on surface plasmon resonance (SPR) signals (as the shift of the reflected light or the change of SPR absorption peak) is taken as the most frequently used sensing indicator in the study of LSPR-enhanced CO_2 sensors. One of the best-reported sensor performances in terms of limit of detection (LOD) of gaseous CO_2 is as low as 10 ppm[18] based on the shift of reflectance associated with SPR signals. However, sensors based upon the change in reflectance lack selectivity, which is one of the critical factors in sensor performance. Therefore, it is advantageous to engage plasmonic materials in IR spectroscopy for a guaranteed high selectivity in applications such as gas sensing because each analyte has its unique IR absorption profile. It is worth mentioning that LSPR-enhanced CO_2 gas sensors normally require two functional layers including a layer of plasmonic material(s) and a layer of sensing material(s) that work side-by-side together, leading the fabrication into a new dimension of complexity.

In this work, we investigated the LSPR effect of a p-type semiconducting chalcogenide material, copper sulfide, on the IR absorption of gases. Instead of detecting a change in bulk refractive index as most LSPR-enhanced sensors, we directly identified IR absorption of gases as the sensing indicator that delivers the addition of characteristic high selectivity and accuracy of IR technique in the sensing platform. The plasmonic material enhances the IR absorption of CO_2 via LSPR. Copper sulfides[35] were chosen for this study for several reasons. First, copper sulfides are a group of low-cost materials that consist of earth-abundant non-toxic elements. Second, copper sulfides can be easily fabricated in thin-film structures that are popular in nanotechnology-enabling applications (e.g., optoelectronics, chemical sensors, etc.) during material synthesis, which simplifies the sensor fabrication process. Third, copper sulfides have been of interest in various optical applications (i.e., photocatalysis[36-38], gas sensing[39], biosensing[40], and solar absorption[41-43]) due to their excellent optical properties including strong LSPR absorption.

Copper sulfides are known as electronic gas sensing materials[44-51] for their electro-conductive nature. Although gas sensing based on the change of electrical conductivity provides relatively high sensitivity and fast response, it comes with a few disadvantages. First, it usually requires additional absorption layer to promote the contact and the chemical reaction between copper sulfides and the analyte. Second, cross-sensitivity can be a significant problem because there are gases that react with copper sulfides more readily and also give a response. Third, there is a potential safety issue by exposing explosive gases (e.g., CH_4, NH_3, and H_2) to electronic sensors. To date, there are limited reports regarding copper sulfides focusing on potential optical applications, a narrow number of which focusing on the utilization of copper sulfide thin films for optical gas sensing, and we cannot find prior reports of this topic for CO_2. One prior study[39] utilized a Pd-coated CuS thin film for optical gas sensing with an effect that is visible to naked eyes. The change of LSPR absorption intensity was used as the sensing indicator to monitor the presence of H_2. This reported sensor provided a LOD of 0.80% for H_2 (i.e., 8,000-ppm H_2).

Copper sulfides exhibit different LSPR by varying stoichiometry between Cu and S[52-54]. Among all the stable phases of copper sulfides at room temperature, the chalcocite Cu_2S shows no LSPR because of the filled valence band, and the covellite CuS exhibits the strongest LSPR resulting from the highest concentration of free carriers in the valence band. Consequently, it is critical to synthesize covellite CuS to achieve high LSPR absorption for optical sensing applications. There are many reported synthesis methods[55-58] for the fabrication of LSPR-possessing copper sulfides. We explored a novel synthesis strategy based on successive ionic layer adsorption and reaction (SILAR)[59, 60] to make CuS thin films because of its sequential growth mechanism. The SILAR provides an easy way to adjust the film thickness by managing the repeating SILAR cycles during the synthesis and is thereby conducive to the study of the influence of film thickness on the opto-electrical properties[61-63] and the sensing enhancement performance of CuS. Moreover, the SILAR offers the advantage of controlling the composition of products by managing the molar concentration ratio of precursors[64]. In this report, we introduced a novel synthesis strategy namely Spatial SILAR that enables a rapid deposition of CuS thin films locally on optical supports.

We facilely prepared covellite CuS thin films on bare microscope glass slides. The performance of CuS-based thin-film sensors for CO_2 was systematically investigated. Based on our knowledge, except the reports by Chong et al.[28, 29] and Chang et al.[65], this work is the only one that conducts a direct gas sensing concept relies on the mechanism of SEIRA spectroscopy based on plasmonic materials. Moreover, the sensing platform proposed in this work surpasses all existing works that use SEIRA to improve gas sensing in terms of the sensor fabrication process and the experimental performance of IR absorption enhancement. Detail comparison with the state-of-the-art works is provided at the end of the Results and Discussion section. The outstanding SEIRA for CO_2 from the sensor is attributed to a dual function of the nanostructured CuS thin film by providing both gas adsorption and LSPR. This unique feature leads to the proximity of adsorbed CO_2 gas molecules with the local field of plasmonic materials. The selectivity of fabricated sensor was verified using Ar and CO_2 gases. An interesting interaction between CuS and gaseous CO_2 was observed via Raman spectroscopy for the first time. A CO_2 sensing mechanism based on LSPR-possessing nanostructured CuS thin film was suggested.

Experimental

Materials and methods

Copper acetate ($Cu(OAc)_2$, Sigma-Aldrich, 98%), thioacetamide (C_2H_5NS, TAA, Sigma-Aldrich, 99%), ethanol (USP, >99.5%), ammonium hydroxide (Macron Fine Chemicals, ACS, 28.0-30.0% as NH_3), and hydrogen peroxide (H_2O_2, EMD Millipore, 30%) were used as purchased without any further purification.

(A)
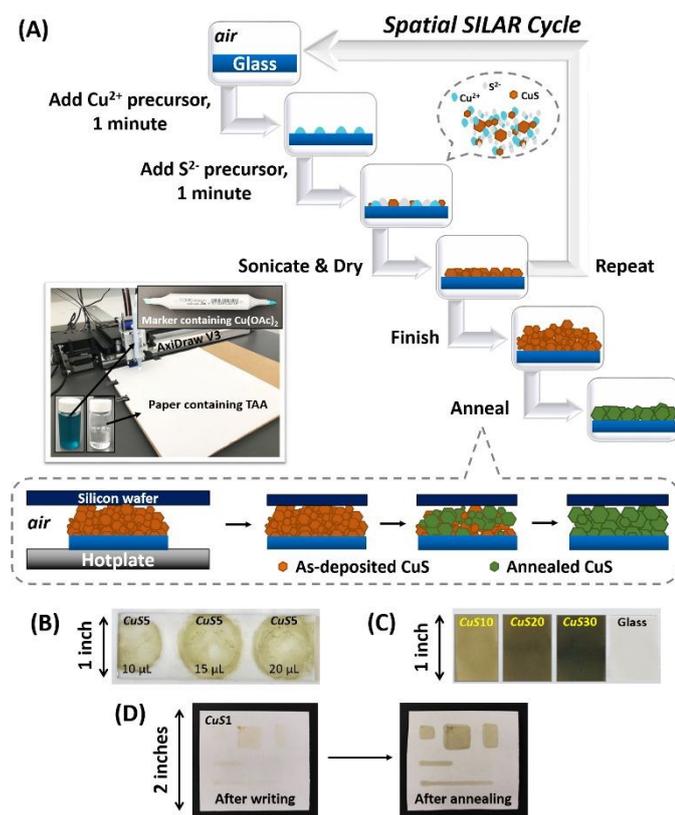
Scheme 1 (A) Schematics of the Spatial SILAR with low-temperature post-annealing. Inserted are optical photos of a lab-designed automatic thin-film fabrication system by AxiDraw V3, and the precursor solutions for CuS. *All materials in the schematics are not in real scale/ratio.* Optical photos of (B) a series of *CuS5* prepared on an untreated glass slide as a control, (C) *CuS10-30* prepared on SC-1-treated glass slides for SEIRA study and a blank glass substrate as reference, and (D) different patterns of *CuS1* written on a piece of standard US letter paper by AxiDraw V3.

99.99+% CO_2 gas and 99.99+% Ar gas were purchased from Airgas (both were taken as 100.00% in the study). Microscope glass slides ($75 \times 25 \times 1.0/0.5$ mm^3) and standard US letter papers were used as substrates for CuS thin-film synthesis, and PELCO® SiO$_2$ support films (40 nm SiO$_2$ membrane, 50×50 μm^2 apertures on 0.5×0.5 mm^2 window, Ø3 mm, TED Pella Inc.) for transmission electron microscope (TEM).

Synthetic procedures

Synthesis of CuS Thin Films on Glass Slides. A piece of microscope glass slide ($75 \times 25 \times 1.0$ mm^3) was cut into four equal pieces. The first step of a standard RCA (Radio Corporation of America) clean, SC-1, was performed on the glass slides with a solution mixture (denoted as RCA solution). RCA solution used in this study contains ammonium hydroxide, hydrogen peroxide, and deionized water (DIW) in a volume ratio of $NH_3:H_2O_2:H_2O$ that equals 1:1:5. Glass slides were cleaned by soap solution and then immersed in RCA solution, subjected to ultrasonication at 70 °C for 1 hour, and followed by rinsing with fresh DIW. Pre-treated substrates were stored in a DIW bath before the deposition of CuS thin films.

Instead of traditional SILAR that includes two washing steps in one SILAR cycle, only one washing step was performed here to accelerate film growth rate. Meanwhile, ultrasonication procedure was

introduced into the washing step to ensure removal of unreacted precursors and any loose particles. Moreover, instead of preparing a batch of solutions for immersing purposes, the precursors were dropwise added onto the substrate surface for green synthesis.

One cycle of standard operating procedure (SOP) of the Spatial SILAR contains the following three steps sequentially (Scheme 1 A):

(1) Drop 300-μL 10-mM Cu(OAc)$_2$ ethanolic solution on a glass substrate, allowing 1 minute for surface bonding, and then drain away excess solution.

(2) Drop 300-μL 10-mM TAA ethanolic solution on the unrinsed substrate, allowing 1 minute for reaction.

(3) Immerse the sample in fresh ethanol and operate ultrasonication for 5 seconds, followed by drying under N$_2$ flow.

Repeat the Spatial SILAR cycle as described above to obtain wanted thickness. The prepared CuS thin films were denoted as *CuSN* in the text, in which **N** is the number of conducted Spatial SILAR cycles.

The molar concentration ratio of the Cu^{2+} and S^{2-} in the precursor solutions was fixed to 1:1 in this study. The whole process of synthesis was carried out under ambient conditions.

After the completion of the Spatial SILAR deposition, the as-deposited CuS thin films were annealed at 85±5 °C for 15 minutes in the air. The color of the thin films changed from brown to olive green after annealing. During the annealing, samples were covered by a silicon wafer to reduce the loss of S, which then was removed after sample temperature naturally cooled down to 35 °C or below. All samples were stored in ambient conditions before characterization and sensing tests.

A series of *CuS5* samples were prepared on an untreated glass slide as a control. Three droplets with different volume (10, 15, and 20 μL, respectively) were added onto the slide sequentially following the SOP of Spatial SILAR.

Synthesis of CuS Thin Films on SiO$_2$ Support Films. Two PELCO® SiO$_2$ support films were rinsed with acetone, methanol, DIW, and ethanol, and dried under N$_2$ flow, sequentially. The same precursor solutions as in the **Synthesis of CuS Thin Films on Glass Slides** were prepared. Two Spatial SILAR cycles were performed on each sample without ultrasonication, but thoroughly rinsed with fresh ethanol. One of the samples was placed on a hot plate with a silicon wafer covered on top of it to assist the low-temperature post-annealing. Both samples were placed in a vacuum chamber for one day before TEM analysis.

Writing CuS on Papers. The same precursor solutions as in the **Synthesis of CuS Thin Films on Glass Slides** were prepared. An empty Copic Sketch marker was used as cartridge to carry the prepared Cu(OAc)$_2$ ethanolic solution. A piece of standard letter paper was soaked in the TAA ethanolic solution for 1 minute, followed by drying under pressed air. The Copic Sketch marker filled with Cu(OAc)$_2$ ethanolic solution was controlled by AxiDraw V3, allowing the precursor to apply onto the prepared TAA paper. The finished paper was then thoroughly rinsed with ethanol without ultrasonication and dried with pressed air. Same post-annealing was performed afterwards.
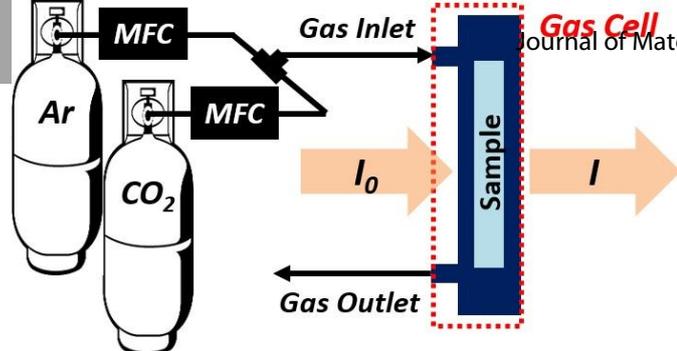
Scheme 2 Schematics of the gas sensing setup. *MFC*: mass flow controller; *I_0*: incident light; *I*: emergent light. *All materials are not in real scale/ratio*.

Synthesis of CuS Powder. Same $Cu(OAc)_2$ and TAA ethanolic solutions as in the **Synthesis of CuS Thin Films on Glass Slides** were prepared as the precursors and well mixed. After agitating the solution mixture for 1 hour, the precipitation was collected through centrifugation. The obtained product was washed with ethanol three times and dried in a vacuum chamber overnight. The powder sample was stored in ambient conditions before TGA.

Study of IR Absorption of CO_2

The optical gas sensing properties of the prepared CuS thin films were studied with a Thermo Scientific Nicolet 6700 FTIR Spectrometer. A customized gas cell with a chamber of 4 mm in thickness was built for FTIR measurement, which was placed in the transmission chamber of the FTIR spectrometer during CO_2 sensing test (Scheme 2). There were two types of samples in this study, of which one was the CuS thin films prepared on glass substrates, and the other one a blank glass substrate as a control. The sample side with CuS thin film was facing the gas phase in the gas cell. The incident light first went through a blank sapphire slide (the fixed window), then the gas phase in the gas cell, the CuS thin film (if there was), and the glass substrate, sequentially, and reached the FTIR detector in the end. All FTIR spectra were collected at room temperature under a flow-through condition in the laboratory. The collection of FTIR spectra was performed after flowing Ar/CO_2 for 3 minutes. Two MFCs were used to control the concentration of CO_2 in a background of Ar in the flowing gas atmosphere.

Characterization

WeWettability analysis of substrates was performed by measurement of water contact angles using a contact angle and surface tension instrument (First Ten Angstroms FTA135 Contact Angle Analyzer) with a 10-µL DIW droplet. The morphologies of the prepared CuS thin films were first analyzed by a Bruker Veeco Innova scanning probe microscope with the tapping mode atomic force microscope (AFM) in a scan range of 10 × 10 µm²; and then by a FEI Quanta 600F Environmental Scanning Electron Microscope (SEM) under high vacuum with approximately 5-nm gold layer on top of the sample, applying an acceleration voltage of 5.00 kV and spot size of 2.5. Film thickness was calculated based on cross-section SEM images. Energy-dispersive X-ray spectroscopy (EDX) system in SEM was conducted to assist the composition determination of the thin films. A FEI Titan 80-200/ChemiSTEM Transmission Electron Microscope (TEM) was used to collect TEM images and Selected Area Electron Diffraction (SAED) patterns. Commercial TEM SiO_2 support films from Ted Pella with 40-nm SiO_2 membrane were used as the

substrate. Average particle sizes were determined by manually counting >100 particles in the micrographs. Thermogravimetric analysis (TGA) was performed by a TA instrument SDT Q600 to investigate the thermal stability of CuS in air and Ar environment, respectively. The phase composition of the chemically synthesized CuS thin films was determined by a Bruker D8 Discover X-ray diffraction (XRD) system operating at 40 kV and 40 mA with Cu k_α radiation of 1.5405 Å in the 2θ scan range from 20° to 50° with a step size of 0.05°. Raman spectra were collected using a WITec Alpha300 RA with an exciting laser wavelength of 514 nm for the analysis of the vibrational modes of the CuS. The absorption spectra of CuS thin films deposited on glass substrates were collected in absorption mode using a JASCO V-670 UV-Vis-NIR spectrophotometer and the Thermo Scientific Nicolet 6700 FTIR Spectrometer used in gas sensing test in attenuated total reflection (ATR) basic smart mode. The electrical properties of prepared CuS thin films were studied with Ecopia Hall Effect Measurement Systems with Four Point Probes (HMS-5000) at room temperature, using 10-step scanning under 1.00-mA current and 0.550-Tesla magnet.

Results and Discussion

SC-1 of RCA clean was carried out on glass slides to remove organic residuals and particles from the substrate, and in the meantime, hydroxylate the surface by attaching OH groups. The obtained hydrophilic surface possesses plenty of reaction sites for the metal species to chemically bond with the substrate surface. The results from contact angle measurements (Figure S-1) confirm the increased hydrophilicity on the glass surface after SC-1, which is favorable for the bonding with hydrophilic metal species, such as Cu^{2+} cations in this study. As such, no additional adhesion layer is necessary to assist the nucleation and growth of CuS thin films. Additionally, no foreign elements are introduced into the reaction. These features are particularly beneficial in optical applications.

As shown in the optical photos in Scheme 1 B and C, *CuS*10, *CuS*20, and *CuS*30 that were prepared on SC-1-treated glass slides present improved uniformity compared with *CuS*5 on an untreated glass slide. All the resulting CuS thin films show excellent adhesion to glass substrates after ultrasonication, revealing no peel-off that is visible to naked eyes as shown in the photos. The observed excellent adhesion suggests that CuS thin films prepared by the Spatial SILAR have the potential for long-term application.

SEM images in Figure S-2 A-C reveal void-free surface coverage of *CuS*10, *CuS*20, and *CuS*30. These SEM images also imply that with more Spatial SILAR cycles, a thicker film with bigger CuS particles could be obtained. Meanwhile, AFM images in Figure S-3 A-F suggest a similar result that both the particle size and the surface roughness increase with increasing Spatial SILAR cycles. The decreased roughness (Figure S-3 G) observed after the low-temperature post-annealing points toward a morphology transformation of the as-deposited CuS thin films during the annealing. The SEM images in Figure 1 A and B present that the as-deposited CuS thin film, which consists of randomly oriented particles with nonuniform size, converts into

ARTICLE
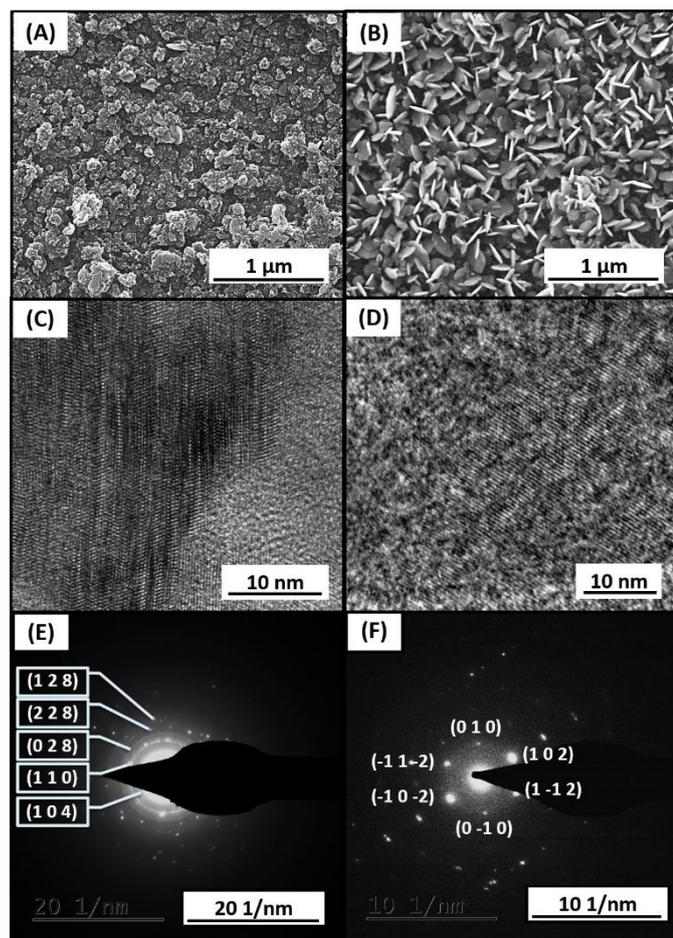
Figure 1 (A, B) SEM and (C, D) TEM images of as-deposited and annealed CuS thin films, respectively, and (E, F) the corresponding SAED patterns.

a film that is packed with CuS nanoflakes after the annealing. This observation indicates a structural phase transition in CuS during the annealing. Additionally, the corresponding TEM images with SAED patterns (Figure 1 C-F) show a tendency that the as-deposited polycrystalline CuS crystals become more defined and uniform, revealing well-defined lattice planes after the annealing.

One explanation for this finding could be a temperature-induced structural transition that brings out a more thermodynamically stable structure for CuS[66, 67]. TGA results (Figure S-4) suggest that CuS starts to lose weight at about 40 °C, which is attributed to the detachment of surface absorbed water[67]. The second weight loss with a faster rate happens at about 80 °C in air, which could be the continuing detachment of physisorbed water coupling with a possible decomposition of CuS due to the loss of S. Although commonly CuS decomposes at a higher temperature than 100 °C[67-69], it is noted that the decomposition temperature could be lower than typical for nanosized CuS[68]. Therefore, the temperature was maintained at 85±5 °C throughout the annealing process to prevent the decomposition from proceeding to a large extent.

Additionally, the samples were covered by a silicon wafer during the post-annealing to limit the loss of S, which is beneficial to retain the preferred stoichiometry of CuS, thereby ensuring

desired high intensity of LSPR absorption to support SEIRA for optical sensing application. Fewer nanoflakes were observed via SEM on a CuS thin film annealed without silicon wafer (Figure S-5 A) than the one with silicon wafer (Figure 1 B). Moreover, as shown in the corresponding EDX results, the atom ratio of Cu to S in the CuS thin film that was annealed without a silicon wafer is 1.127:1 (Figure S-5 B), while the one annealed with silicon wafer is 1.017:1 (Figure S-5 D). Therefore, it is reasonable to assume that due to the restraint from the silicon wafer more released S would stay close to the remaining CuS on the substrate, subject to a reaction that promotes the structural transition. Both the reaction between S and CuS and the structural transition occur continuously throughout the annealing process owing to the induced heat, resulting in the structural phase transition in CuS that leads to the formation of hexagonal CuS nanoflakes. It is also discovered by EDX that the stoichiometric ratio between Cu and S in the as-deposited CuS thin film is 0.938:1 (Figure S-5 C), which is smaller than the stoichiometric ratio of CuS that is 1:1. This is possibly owing to the attachment of excess S species on the surface. After the low-temperature annealing, the atom ratio of Cu to S increases to 1.017:1, indicating the detachment of S as a result of annealing.

XRD results presents no prominent diffraction peaks for CuS as shown in Figure S-6, which is possibly due to nanocrystallinity and small quantity. We used Raman analysis to provide additional structural data for these Spatial SILAR-prepared CuS thin films. Raman spectra (Figure S-7) show an evident peak at approximately 468 cm^{-1} that is associated with the vibrational mode of S–S bond, while an inconspicuous peak at around 259 cm^{-1} related to that of the Cu-S bond[70], and the peak at about 920 cm^{-1} is identified in covellite CuS via RRUFF database (RRUFF ID: R060143.4). Regardless of the number of conducted Spatial SILAR cycles or the conduction of post-annealing, there is no observation on shifting of Raman peaks, indicating that all the samples are covellite CuS. Therefore, it suggests that the Spatial SILAR with controlled annealing process can achieve efficient deposition of covellite CuS thin films as long as the molar concentration ratio of the precursors is fixed. At this point, we confirm that covellite CuS thin films, which exhibits the most substantial LSPR absorption among all the compositions of copper sulfides, are obtained via the Spatial SILAR and achieved nanoflake-structure after a controlled low-temperature post-annealing without compromising the desired stoichiometry.

The optical properties of CuS thin films were investigated by Vis-NIR and FTIR spectroscopies. We noticed in the NIR absorption spectra (Figure S-8) that all the synthesized CuS thin films show a broad LSPR absorption that possibly absorbs SWIR/MIR other than a narrow absorption that is usually located in the NIR region[35, 52, 53, 55-58, 71]. The broad LSPR absorption generating from the nanostructured CuS thin films becomes stronger with more synthesis cycles (resulting in thicker film) and the low-temperature post-annealing (resulting in nanoflake-structure with better crystallinity). As shown in Figure 2, the FTIR absorption spectra of the CuS thin films suggest a broad MIR absorption. Additionally, it is interestingly noticed that there is

ARTICLE
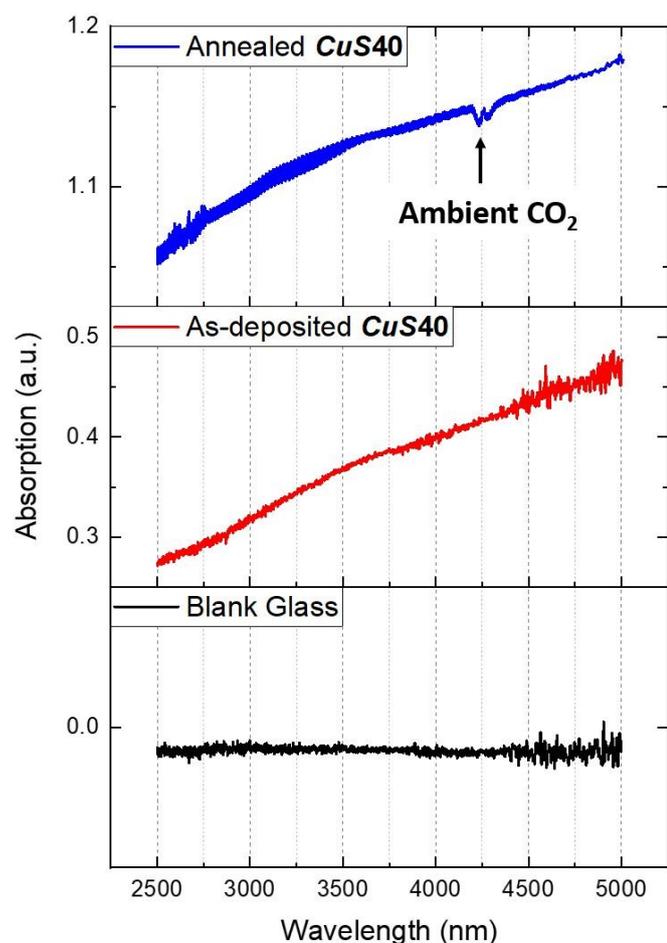
Figure 2 FTIR ATR absorption spectra of as-deposited and annealed *CuS*40, and a blank glass substrate measured under standard ambient conditions.

a pair of CO_2 absorption bands in the spectrum of annealed *CuS*40, while no such absorption bands in that of as-deposited *CuS*40 nor a blank glass substrate. This observation indicates that under standard ambient conditions (approximately 1 atm, 20 °C, 55-70% humidity) there is likely an adsorption of ambient CO_2 in the annealed CuS thin film consisting of hexagonal nanoflakes. The results from these absorption spectra confirm that the broad LSPR absorption from the CuS thin film synthesized by the Spatial SILAR covers both NIR and MIR ranges. This property renders the CuS thin film suitable for enhancing the IR absorption of CO_2 in both NIR and MIR ranges. The increased LSPR absorption intensity acquired by the annealed CuS thin films is likely attributed to increased free carrier concentration[72], which is associated with the improved crystallinity and the increased surface area. The results from XRD and Raman characterization indicate an increased crystallinity of these thin films after the annealing. As observed *via* SEM, the as-deposited thin films consist of randomly oriented intergrown particles, while the annealed ones exhibit structure constructed by nanoflakes, suggesting an increase in accessible surface area. Results from Hall Effect measurements (Figure S-9) confirm a significantly increased electrical conductivity of annealed CuS thin films that corresponds to the

increased free carrier concentration in these films, contributing to the favorable strong LSPR absorption[72] for SEIRA.

The selectivity of the proposed CuS-based IR gas sensing platform in this study is demonstrated by using Ar and CO_2 as the analytes. As shown in the as-collected FTIR transmission spectra of Ar and CO_2 in Figure S-10 A, there is no absorption of Ar in SWIR range, while the characteristic absorption bands of CO_2 are observed. Because of the unique IR absorption profile of each analyte, the selectivity and accuracy of this IR gas sensing platform are guaranteed. Indicated by the results from these FTIR spectra, intrinsically the glass substrate absorbs 23-35% SWIR, while the *CuS*50 prepared on such glass substrate absorbs over 99% SWIR. There is no shift nor shape-varying of the CO_2 absorption bands observed after applying CuS, only different absorption intensity. Moreover, the analyte(s) (i.e., Ar/CO_2 with varying concentration) has no influence on the intrinsic LSPR absorption of CuS.

The CO_2 IR absorption profile of interest is obtained based on Beer-Lambert Law. The calculation method is detailed described in a previous work[29]. With the calculation, the influence of the intrinsic absorption from both the substrate and the CuS thin film can be eliminated, leaving only the IR absorption of CO_2 in the profile. The calculated CO_2 IR absorption profile under different conditions are displayed as the FTIR transmission spectra in Figures S-10 B, S-11 A-D, and S-12.

As shown in Figure S-10 B, the as-deposited *CuS*50 barely enhances the IR absorption of CO_2 compared to the annealed one, which is likely due to its structural differences and the insignificant LSPR absorption as observed *via* SEM and IR spectroscopies, respectively. Therefore, in the study, we only focused on the sensing enhancement performance of annealed CuS thin films. It is noted that the Fabry–Pérot (FP) effect is a dominant optical interference when the intrinsic light absorption of the sensor is significant or that of the analyte is weak. The two surfaces of a regular glass slide serve as two reflective glass optical flats, resulting in the multiple interference peaks observed in the FTIR spectra (e.g., Figure S-11 C), visualizing the presence of FP effect. According to the CO_2 IR absorption enhancement shown in Figure S-11 E, *CuS*30 provides a more stable and more considerable IR absorption enhancement for CO_2 than *CuS*10 or *CuS*20. However, when the absorption from CO_2 becomes weak due to a low concentration, the multiple interference peaks from the FP effect conceal the absorption bands of CO_2, which dysfunctions the sensor. Therefore, thinner glass slides (0.5-mm thick) were chosen as substrates in the following study, which is efficient to reduce the inner reflection, and thereby weaken the FP effect. *CuS*40 was prepared on this thin slide accordingly and obtained sufficient LSPR for SEIRA (Figure S-8).

The CO_2 concentration used for gas sensing test on *CuS*40 ranges from 0.01% to 2.00% (i.e., 100 ppm to 20,000 ppm), which reaches the lower limitation based on the MFCs. Plots of experimental IR absorption coefficient of CO_2 as a function of concentration are shown in Figures 3 A, and S-13, of which the values are small in the SWIR region as expected. Adopting the definition of enhancement factor (*EF*) used in our previous

(A)

(B)
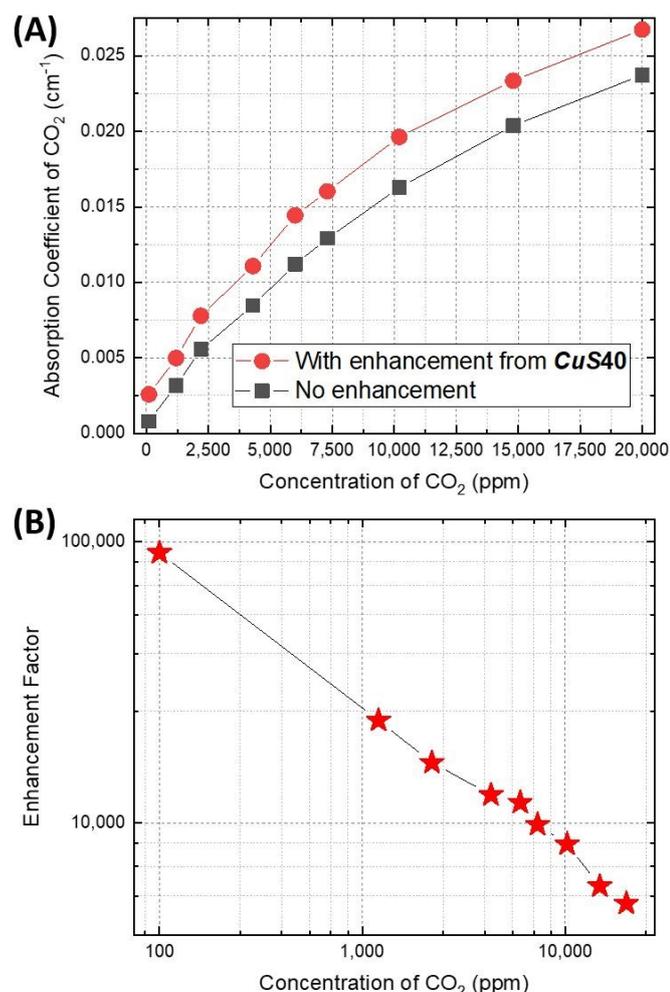
Figure 3 (A) Experimental IR absorption coefficient of CO_2 (at approximately 2683 cm^{-1}) as a function of concentration, obtained with/without the enhancement from **CuS40**. (B) Calculated IR absorption enhancement factor for CO_2 provided by **CuS40**.

works[28, 29, 73], we determined the sensing enhancement performance as the equivalent optical path length provided by nm-thick plasmonic thin-film materials in this work.

The experimental IR absorption coefficient of CO_2 (Figures 3 A) indicates a constant increase when applying **CuS40** in the sensor, whereas the increase is slightly larger at high CO_2 concentration than at low concentration. However, the enhanced absorption coefficient of CO_2 provided by **CuS40** significantly exceeds its intrinsic absorption coefficient when the concentration is as low as 100 ppm. The calculated *EF* for IR absorption of CO_2 provided by **CuS40** is shown in Figure 3 B. It states a nonlinear relationship of *EF* as a function of CO_2 concentration, which is small at high CO_2 concentration and big at low concentration. This nonlinear relationship is likely a result of different CO_2 concentration ratios between the CO_2 on CuS surface and CO_2 in the gas phase at high and low CO_2 concentration in the gas phase, which is dominated by different enhancement elements. At high CO_2 level, where the adsorption is the dominant enhancement element, a smaller percentage of CO_2 molecules are under the electric field near the surface of CuS nanoflakes; thus, the smaller *EF*. At lower total CO_2 level, where the LSPR effect is the dominant

(A)

(B)
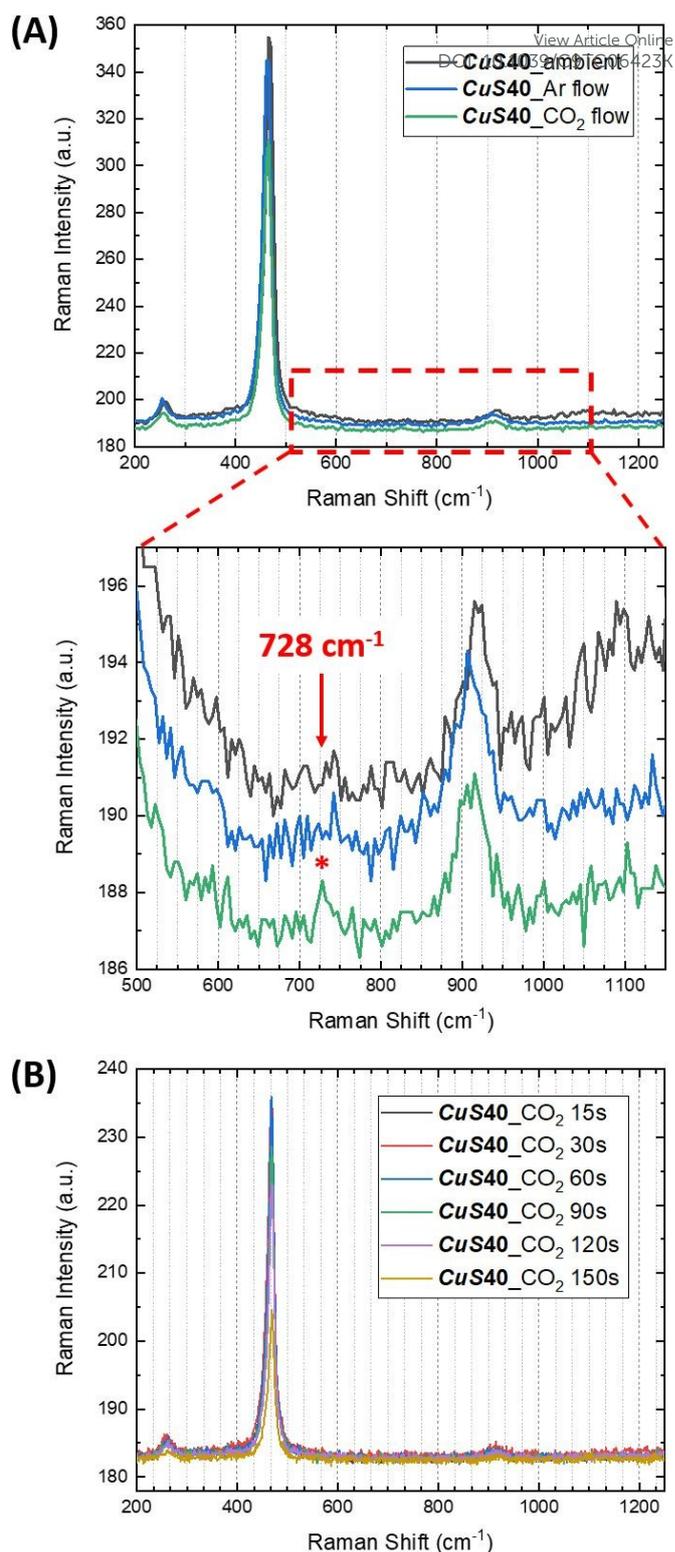
Figure 4 (A) Raman spectra of annealed **CuS40** collected under standard ambient conditions, and the *in-situ* measurement while flowing Ar (100.00%) and CO_2 (100.00%), respectively; and a magnified view for the selected area indicated by the red dash line. (B) *In-situ* Raman spectra of annealed **CuS40** collected after exposing to a flow of CO_2 for different time (in seconds).

enhancement element, a higher percentage of CO_2 molecules are on the surface of CuS, which then result in a more substantial *EF*.

The obtained *EF* results indicate the highest IR absorption enhancement for 100-ppm CO_2 is over 90,000-fold. Such substantial enhancement can be attributed to the combination of LSPR effect and the structure of covellite CuS-nanoflake thin film. First, the free carriers in CuS nanoflake oscillate due to the electromagnetic field and resonate at the LSPR condition, thereby providing a large electromagnetic field in the surface proximity[74, 75]. Molecules with active IR vibrations are likely to receive intensified vibration if entering this intense electromagnetic field[76]. The ultrahigh free carrier concentration of the annealed CuS thin film fabricated by the Spatial SILAR with controlled post-annealing treatment can contribute to an intense and localized electromagnetic field[72] as evidently shown *via* the LSPR absorption spectra (Figure S-8). The nanoflake structure also provides a more accessible surface to interact with the CO_2 molecules.

The interaction between CuS and CO_2 was studied *in-situ* using a Raman spectrometer. As shown in Figure 4 A, all three characteristic Raman peaks of CuS shift to smaller wavenumbers (approximately 10 cm^{-1} difference) while flowing gases over the surface of **CuS40** in an open environment under standard ambient conditions. An identical shift is observed with both Ar flow and CO_2 flow. A red-shift on Raman peak can result from material lattice expansion or other effects such as phonon confinement[77]. Other than the red-shift, there is no observation of any new peak when flowing Ar. However, there is a new peak appeared at approximately 728 cm^{-1} when flowing CO_2, which disappeared after stopping the CO_2 flow. This peak position matches with the stretching mode of C-S bond[78] that is possibly formed between C in CO_2 and S in CuS. This result indicates a close interaction between the sulfur-rich covellite CuS and CO_2 molecules, where the surface sulfur sites could potentially promote adsorption of CO_2 and contribute to the high sensitivity towards CO_2. Furthermore, it is found that the Raman peak intensities, including S-S and Cu-S bonds, decreases as exposing to CO_2 for longer time (Figure 4 B). This result suggests the interaction CO_2 with CuS might alter the electron-phonon scattering rate[79] in CuS. Such interaction is reversible and does not influence the intrinsic absorption profile of CuS nor that of CO_2, as shown in the FTIR spectra. This close interaction, however, is likely another essential factor for significant enhancement.

In comparison with the state-of-the-art works, the absorption coefficient of 100-ppm CO_2 in the 4-mm thick gas cell used in this study is around 7.95×10^{-4} /cm, which is about 20 times smaller than that measured from a 5-cm single-mode fibre (SMF)[73]. However, the *EF* for 100-ppm CO_2 in this work is 91,467, which is about 281 times higher than that from the metal-organic framework (MOF)-coated SMF. This result envisions a future to apply CuS on optical structures with a larger unit sensing area (e.g., optical fibres) to potentially receive an enlarged enhancement. Later on, a novel integrated sensor[28] of MOF-coated Au-NPA on suspended Si_3N_4 achieves an ultrahigh plasmonic field that reaches a low LOD of 7,300 ppm for CO_2 with a high IR absorption *EF* that is 1620 while the active sensing area is only 4.00×10^{-4} cm^2. Recently another integrated sensor based on a microstructured photonic crystal[65]

is reported, which functions under elevated temperature and uses SEIRA for direct gas sensing. This sensor provides 14 times enhancement of the IR absorption signal for CO_2. The single-material thin-film sensor reported in this work offers the highest *EF* for low-concentration CO_2, surpassing all existing works that use SEIRA for gas sensing. Moreover, the nanostructured CuS was fabricated *via* a novel and facile process, Spatial SILAR, which can be implemented in a direct-write manner.

Conclusions

In conclusion, this work presents the first demonstration that utilizes CuS solely for SEIRA of CO_2, portraying a promising future in the development of chip-scale IR sensors for distributed sensing. In this work, covellite CuS thin films that exhibit substantial LSPR absorption were successfully synthesized *via* the Spatial SILAR at room temperature with a mild post-annealing. This novel synthesis strategy provides a rapid fabrication of thin films with a controllable scale. The resulting CuS thin films were comprising of nanoflakes after the low-temperature post-annealing. The influence of film thickness on SEIRA of CO_2 was studied. It was found that thicker CuS thin film provides more considerable enhancement, although the enhancement can be compromised by the intrinsic strong light absorption from the increased thickness, indicating that there is an optimal thickness for CuS thin film in such optical application. In this study, CuS-based thin-film sensor prepared by 40 Spatial SILAR cycles offered an optimal sensing conditions and provided excellent SEIRA of CO_2. A low experimental detection limit of 100 ppm for CO_2 with over 9×10^4-fold enhancement was achieved, which is the best result among current reported LSPR-enhanced CO_2 IR sensors. The significant SEIRA of CO_2 has likely attributed to both the LSPR effect from covellite CuS and the strong CO_2 interaction with the nanoflakes-constructed thin film. A close relationship between CO_2 and sulfur-rich covellite CuS was observed *via* Raman spectroscopy for the first time, which is likely another essential factor for the significant enhancement.

In summary, the nanostructured CuS thin film *via* the Spatial SILAR process shows significant SEIRA of CO_2, which offers considerable prospective value to serve in various fields, such as transportations, electricity generation plants, and other high-standard gas monitoring systems.

Conflicts of interest

There are no conflicts to declare.

Acknowledgements

Notes and references

1   O. S. Board and N. R. Council, *Ocean acidification: a national strategy to meet the challenges of a changing ocean*, National Academies Press, 2010.

2   R. Govindan, A. Korre, S. Durucan and C. E. Imrie, *International Journal of Greenhouse Gas Control*, 2011, **5**, 589-597.

3   C. Schutze, P. Dietrich and U. Sauer, *International Journal of Greenhouse Gas Control*, 2013, **18**, 285-295.

4   J. Jiang, M. D. Steven, R. He, Y. Chen, P. Du and H. Guo, *International Journal of Greenhouse Gas Control*, 2015, **37**, 1-11.

5   K. Harris, D. White, D. Melanson, C. Samson and T. M. Daley, *International Journal of Greenhouse Gas Control*, 2016, **50**, 248-260.

6   J. Jiang, M. D. Steven, R. He, Y. Chen and P. Du, *Energy*, 2016, **100**, 73-81.

7   P. Kumar and K.-H. Kim, *Applied Energy*, 2016, **172**, 383-397.

8   S. Wang, J. San, J. Yu, R. Lee and N. Liu, *International Journal of Greenhouse Gas Control*, 2016, **55**, 202-208.

9   K. Harris, D. White and C. Samson, *Geophysics*, 2017, **82**, M81-M96.

10   X. Liu, S. Cheng, H. Liu, S. Hu, D. Zhang and H. Ning, *Sensors (Basel, Switzerland)*, 2012, **12**, 9635-9665.

11   P.-S. Wei, Y.-C. Hsieh, H.-H. Chiu, D.-L. Yen, C. Lee, Y.-C. Tsai and T.-C. Ting, *Heliyon*, 2018, **4**, e00785.

12   K.-J. Kim, P. Lu, J. T. Culp and P. R. Ohodnicki, *ACS Sensors*, 2018, **3**, 386-394.

13   A. Hartstein, J. Kirtley and J. Tsang, *Physical Review Letters*, 1980, **45**, 201.

14   N. Nath and A. Chilkoti, *Analytical Chemistry*, 2004, **76**, 5370-5378.

15   K. Göeken, T. Brinkman, L. Segerink, T. Oude-Munnink, R. Gill and A. Andreski, *Multidisciplinary Digital Publishing Institute Proceedings*, 2017, **1**, 815.

16   S. Herminjard, L. Sirigu, H. P. Herzig, E. Studemann, A. Crottini, J. P. Pellaux, T. Gresch, M. Fischer and J. Faist, *Optics express*, 2009, **17**, 293-303.

17   L. E. Kreno, J. T. Hupp and R. P. Van Duyne, *Analytical Chemistry*, 2010, **82**, 8042-8046.

18   T. Lang, T. Hirsch, C. Fenzl, F. Brandl and O. S. Wolfbeis, *Analytical Chemistry*, 2012, **84**, 9085-9088.

19   A. Abdelhalim, A. Abdellah, G. Scarpa and P. Lugli, *Nanotechnology*, 2014, **25**, 10.

20   F. A. A. Nugroho, C. Xu, N. Hedin and C. Langhammer, *Analytical Chemistry*, 2015, **87**, 10161-10165.

21   A. Pusch, A. De Luca, S. S. Oh, S. Wuestner, T. Roschuk, Y. G. Chen, S. Boual, Z. Ali, C. C. Phillips, M. H. Hong, S. A. Maier, F. Udrea, R. H. Hopper and O. Hess, *Scientific Reports*, 2015, **5**, 7.

22   T. Allsop, R. Arif, R. Neal, K. Kalli, V. Kundrat, A. Rozhin, P. Culverhouse and D. J. Webb, *Light: Science and Applications*, 2016, **5**, 8.

23   E. Fagadar-Cosma, A. Lascu, A. Palade, I. Creanga, G. Fagadar-Cosma and M. Birdeanu, *Digest Journal of Nanomaterials and Biostructures*, 2016, **11**, 419-424.

24   R. Nuryadi and R. D. Mayasari, *Applied Physics A: Materials Science and Processing*, 2016, **122**, 6.

25   E. A. Hurtado-Aviles, J. A. Torres, M. Trejo-Valdez, G. Urriolagoitia-Sosa, I. Villalpando and C. Torres-Torres, *Micromachines*, 2017, **8**, 321.

26   V. Lirtsman, M. Golosovsky and D. Davidov, *Review of Scientific Instruments*, 2017, **88**, 7.

27   S. Y. Tseng, S. Y. Li, S. Y. Yi, A. Y. Sun, D. Y. Gao and D. H. Wan, *ACS Applied Materials & Interfaces*, 2017, **9**, 17307-17317.

28   X. Y. Chong, Y. J. Zhang, E. W. Li, K. J. Kim, P. R. Ohodnicki, C. H. Chang and A. X. Wang, *ACS Sensors*, 2018, **3**, 230-238.

29   X. Chong, K.-j. Kim, Y. Zhang, E. Li, P. R. Ohodnicki, C.-H. Chang and A. X. Wang, *Nanotechnology*, 2017, **28**, 26LT01.

30   K.-J. Kim, X. Chong, P. B. Kreider, G. Ma, P. R. Ohodnicki, J. P. Baltrus, A. X. Wang and C.-H. Chang, *Journal of Materials Chemistry C*, 2015, **3**, 2763-2767.

31   D. Kitenge, R. K. Joshi, M. Hirai and A. Kumar, *IEEE Sensors Journal*, 2009, **9**, 1797-1801.

32   P. J. Rodriguez-Canto, M. Martinez-Marco, F. J. Rodriguez-Fortuno, B. Tomas-Navarro, R. Ortuno, S. Peransi-Llopis and A. Martinez, *Optics express*, 2011, **19**, 7664-7672.

33   V. A. G. Rivera, F. A. Ferri and E. M. Jr, in *Plasmonics - Principles and Applications*, ed. K. Y. Kim, InTech, Rijeka, 2012, DOI: 10.5772/50753, p. Ch. 11.

34   M. Sturaro, E. D. Gaspera, C. Cantalini, M. Guglielmi and A. Martucci, *Proceedings*, 2017, **1**, 319.

35   Y. Liu, M. Liu and M. T. Swihart, *The Journal of Physical Chemistry C*, 2017, **121**, 13435-13447.

36   Z. Cheng, S. Wang, Q. Wang and B. Geng, *CrystEngComm*, 2010, **12**, 144-149.

37   P. Kar, S. Farsinezhad, X. Zhang and K. Shankar, *Nanoscale*, 2014, **6**, 14305-14318.

38   A. Manzi, T. Simon, C. Sonnleitner, M. Döblinger, R. Wyrwich, O. Stern, J. K. Stolarczyk and J. Feldmann, *Journal of the American Chemical Society*, 2015, **137**, 14007-14010.

39   S. S. Kalanur, Y.-A. Lee and H. Seo, *RSC Advances*, 2015, **5**, 9028-9034.

40   H. Nishi, K. Asami and T. Tatsuma, *Optical Materials Express*, 2016, **6**, 1043-1048.

41   J. A. Bragagnolo, A. M. Barnett, J. E. Phillips, R. B. Hall, A. Rothwarf and J. D. Meakin, *IEEE Transactions on electron devices*, 1980, **27**, 645-651.

42   M. Page, O. Niitsoo, Y. Itzhaik, D. Cahen and G. Hodes, *Energy & Environmental Science*, 2009, **2**, 220-223.

43   F. Tao, Y. Zhang, K. Yin, S. Cao, X. Chang, Y. Lei, D. S. Wang, R. Fan, L. Dong and Y. Yin, *ACS applied materials & interfaces*, 2018, **10**, 35154-35163.

44   A. Galdikas, A. Mironas, V. Strazdien, A. Šetkus, I. Ancutien and V. Janickis, *Sensors and Actuators B: Chemical*, 2000, **67**, 76-83.

45   A. Šetkus, A. Galdikas, A. Mironas, I. Šimkiene, I. Ancutiene, V. Janickis, S. Kaciulis, G. Mattogno and G. Ingo, *Thin Solid Films*, 2001, **391**, 275-281.

46   A. Šetkus, A. Galdikas, A. Mironas, V. Strazdien, I. Šimkien, I. Ancutien, V. Janickis, S. Kačiulis, G. Mattogno and G. Ingo, *Sensors and Actuators B: Chemical*, 2001, **78**, 208-215.

47   A. A. Sagade and R. Sharma, *Sensors and Actuators B: Chemical*, 2008, **133**, 135-143.

48   M. S. Shinde, D. R. Patil and R. S. Patil, *Indian Journal of Pure & Applied Physics*, 2013, **51**, 713-716.

49   J. Xu, J. Zhang, C. Yao and H. Dong, *Journal of the Chilean Chemical Society*, 2013, **58**, 1722-1724.

50   F. A. Sabah, N. M. Ahmed, Z. Hassan and H. S. Rasheed, *Sensors and Actuators A: Physical*, 2016, **249**, 68-76.

51 U. Shamraiz, R. A. Hussain and A. Badshah, *Journal of Solid State Chemistry*, 2016, **238**, 25-40.

52 Y. Xie, A. Riedinger, M. Prato, A. Casu, A. Genovese, P. Guardia, S. Sottini, C. Sangregorio, K. Miszta and S. Ghosh, *Journal of the American Chemical Society*, 2013, **135**, 17630-17637.

53 M. Brelle, C. Torres-Martinez, J. McNulty, R. Mehra and J. Zhang, *Pure and applied chemistry*, 2000, **72**, 101-117.

54 S.-W. Hsu, W. Bryks and A. R. Tao, *Chemistry of Materials*, 2012, **24**, 3765-3771.

55 M. Zhou, R. Zhang, M. Huang, W. Lu, S. Song, M. P. Melancon, M. Tian, D. Liang and C. Li, *Journal of the American Chemical Society*, 2010, **132**, 15351-15358.

56 M. Kruszynska, H. Borchert, A. Bachmatiuk, M. H. Rümmeli, B. Büchner, J. r. Parisi and J. Kolny-Olesiak, *ACS Nano*, 2012, **6**, 5889-5896.

57 K. Ren, P. Yin, Y. Zhou, X. Cao, C. Dong, L. Cui, H. Liu and X. Du, *Small*, 2017, **13**, 1700867.

58 W. van der Stam, S. Gudjonsdottir, W. H. Evers and A. J. Houtepen, *Journal of the American Chemical Society*, 2017, **139**, 13208-13217.

59 H. Pathan and C. Lokhande, *Bulletin of Materials Science*, 2004, **27**, 85-111.

60 T. Ç. Taşdemirci, *Vacuum*, 2019.

61 T. Ç. Taşdemirci, *Optical and Quantum Electronics*, 2019, **51**, 245.

62 Y. Akaltun and T. Çayır, *Journal of Alloys and compounds*, 2015, **625**, 144-148.

63 T. Ç. Taşdemirci, *Chemical Physics Letters*, 2020, **738**, 136884.

64 T. Ç. Taşdemirci, *Journal of Scientific Perspectives*, 2019, **3**, 207-214.

65 Y. Chang, D. Hasan, B. Dong, J. Wei, Y. Ma, G. Zhou, K. W. Ang and C. Lee, *ACS applied materials & interfaces*, 2018, **10**, 38272-38279.

66 Á. Morales-García, J. He, A. L. Soares and H. A. Duarte, *CrystEngComm*, 2017, **19**, 3078-3084.

67 Y. L. Auyoong, P. L. Yap, X. Huang and S. B. A. Hamid, *Chemistry Central Journal*, 2013, **7**, 67.

68 S. Chaki, J. P. Tailor and M. Deshpande, *Journal of Thermal Analysis and Calorimetry*, 2014, **117**, 1137-1144.

69 M. Nafees, M. Ikram and S. Ali, *Digest Journal of Nanomaterials and Biostructures*, 2015, **10**, 635-641.

70 A. G. Milekhin, N. A. Yeryukov, L. L. Sveshnikova, T. A. Duda, E. E. Rodyakina, V. A. Gridchin, E. S. Sheremet and D. R. Zahn, *Beilstein journal of nanotechnology*, 2015, **6**, 749.

71 S. S. Kalanur and H. Seo, *RSC Advances*, 2017, **7**, 11118-11122.

72 J. M. Luther, P. K. Jain, T. Ewers and A. P. Alivisatos, *Nature materials*, 2011, **10**, 361.

73 X. Chong, K.-J. Kim, E. Li, Y. Zhang, P. R. Ohodnicki, C.-H. Chang and A. X. Wang, *Sensors and Actuators B: Chemical*, 2016, **232**, 43-51.

74 K. A. Willets and R. P. Van Duyne, *Annual Review of Physical Chemistry*, 2007, **58**, 267-297.

75 K. M. Mayer and J. H. Hafner, *Chemical reviews*, 2011, **111**, 3828-3857.

76 F. Neubrech and A. Pucci, *IEEE Journal of selected topics in quantum electronics*, 2013, **19**, 4600809-4600809.

77 O. Yassin, S. Alamri and A. Joraid, *Journal of Physics D: Applied Physics*, 2013, **46**, 235301.

78 F. Bensebaa, Y. Zhou, A. Brolo, D. Irish, Y. Deslandes, E. Kruus and T. Ellis, *Spectrochimica Acta Part A: Molecular and Biomolecular Spectroscopy*, 1999, **55**, 1229-1236.

79 C. Casiraghi, *Physical Review B*, 2009, **80**, 233407.